nature neuroscience

Supplementary information

https://doi.org/10.1038/s41593-025-01961-y

Noninvasive reduction of neural rigidity alters autistic behaviors in humans

In the format provided by the authors and unedited

Supplementary Information

Contents

Abbreviations and acronyms

Abbreviations	Meaning	Misc
ADHD	Attention deficit hyperactivity disorder	
ADOS	Autism Diagnostic Observation Schedule	ADOS-2 was used here.
AN	auditory network	
ASD	autism spectrum disorder	
BDNS	brain-state-driven neural stimulation	
CON	cingulo-opercular network	
DAN	dorsal attention network	
DMN	default mode network	
FPN	frontoparietal network	
MEM	Maximum entropy model	
NVJ	Nonverbal-information-based judgement	A term specific to this study
SAN	salience network	
SMN	somatosensory network	
SPL	superior parietal lobule	
TD	typically developing	
TMS	transcranial magnetic stimulation	
VAN	ventral attention network	
VN	visual network	

Specific terms with specific meanings in this study

Atypical nonverbal information processing	Quantified as the number of nonverbal-information-based judgements (NVJ) in the friend-or-foe judgement test.
Cognitive inflexibility	Quantified as the task-repetition length in the spontaneous task-switching test.
Indirect transition frequency	Frequency of the brain state transitions between the two major states via either of the two minor states.
Neural rigidity	Quantified as indirect transition frequency.
Perceptual overstability	Quantified as the perceptual duration in the test of the bistable visual perception.

Supplementary Figures

Supplementary Fig. 1

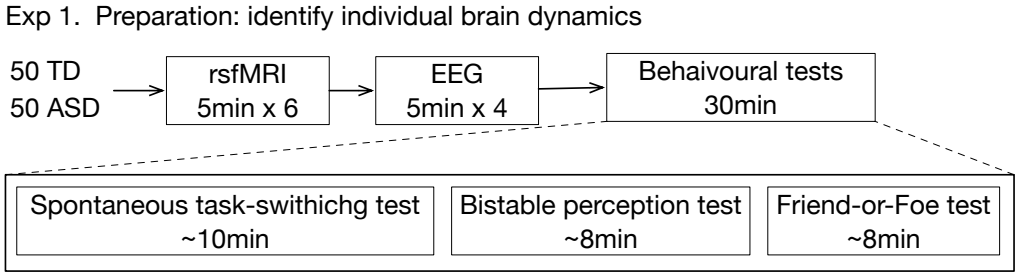

Supplementary Fig. 1. **The design of Experiment 1.** We collected rsfMRI data and resting-state EEG data from the 50 high-functioning ASD and 50 TD individuals to assess their baseline brain dynamics and tune EEG preprocessing parameters for the following BDNS experiments. After the recordings, we also collected behavioural responses to the three different psychological tests.

Supplementary Fig. 2

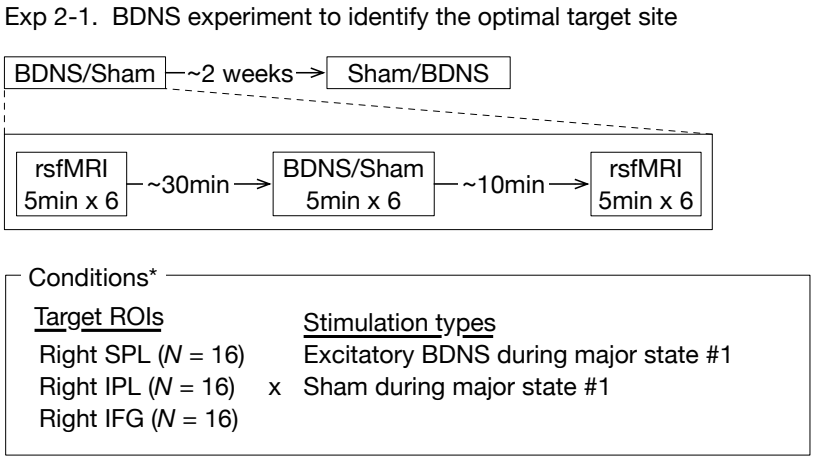

* One of the target ROIs was randomly assigned to 48 of the 50 participants with ASD. The 48 participants were also randomly chosen from the 50 autistic participants. The order of the BDNS and Sham conditions was pseudo-randomly set across participants.

Supplementary Fig. 2. Design of Experiment 2-1. We performed a sham-controlled BDNS experiment employing the 50 ASD individuals and compared the neural effect (i.e., the indirect transition frequency) between the three FPN regions.

Supplementary Fig. 3

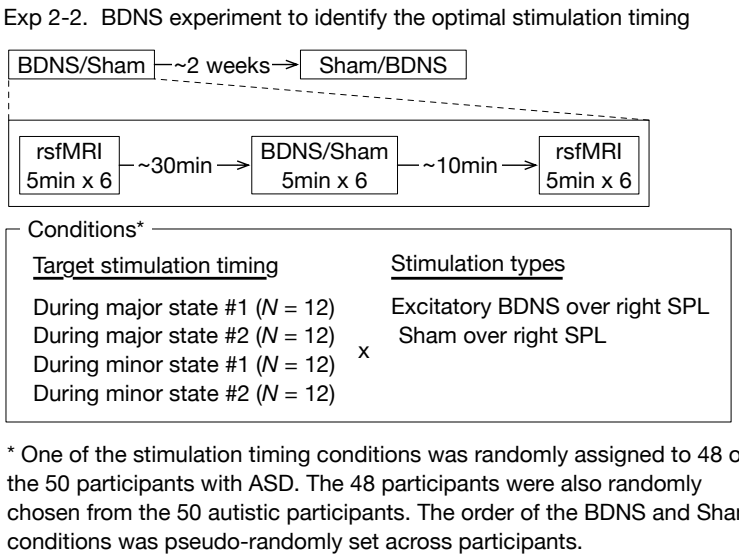

* One of the stimulation timing conditions was randomly assigned to 48 of the 50 participants with ASD. The 48 participants were also randomly chosen from the 50 autistic participants. The order of the BDNS and Sham conditions was pseudo-randomly set across participants.

Supplementary Fig. 3. **Design of Experiment 2-2.** We conducted another sham-controlled BDNS experiment and compared the neural effect between four different BDNS timings.

Supplementary Fig. 4

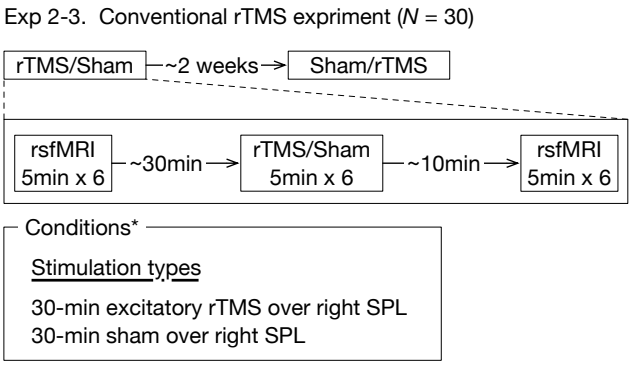

* The order of the rTMS and Sham conditions was pseudo-randomly set across participants. This experiment employed 30 ASD participants, who were randomly chosen from the 50 partcipants.

Supplementary Fig. 4. **Design of Experiment 2-3.** As a control, we examined behavioural effects of a conventional repetitive TMS over the same SPL.

Supplementary Fig. 5

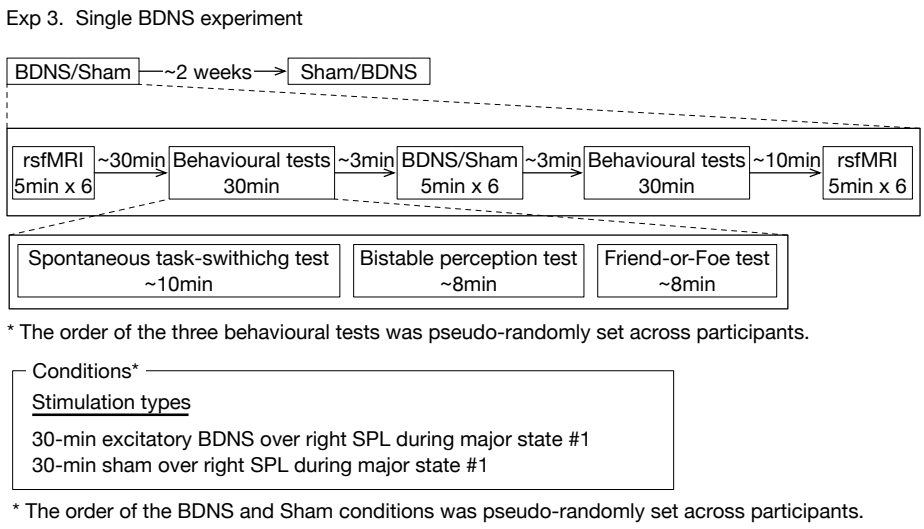

Supplementary Fig. 5. **Design of Experiment 3**. In this single-session BDNS experiment, we examined behavioural effects of the optimised BDNS.

Supplementary Fig. 6

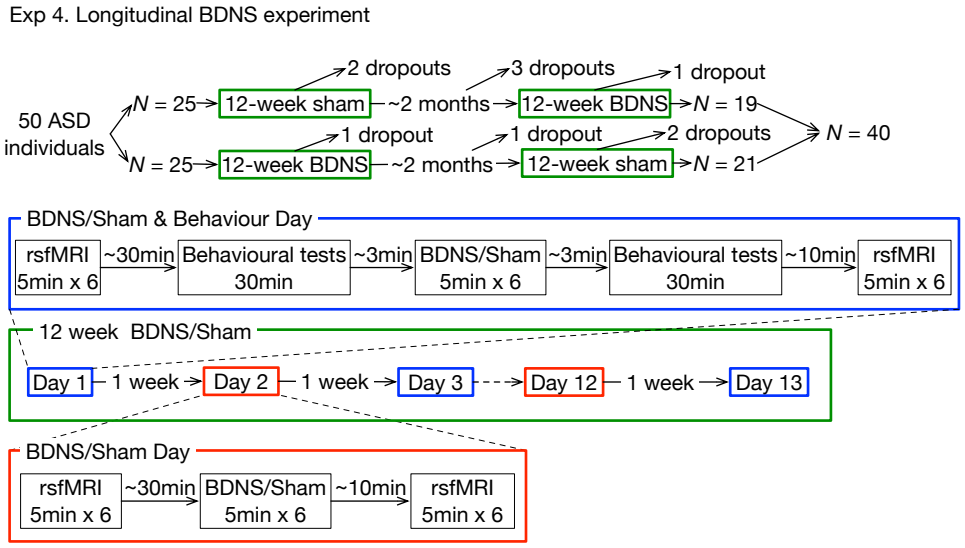

Supplementary Fig. 6. **Design of Experiment 4: longitudinal BDNS experiment**. We adopted a sham-controlled cross-over design. The participants underwent weekly BDNS/sham sessions and rsfMRI scans. We examined their behavioural performance bi-weekly.

Supplementary Fig. 7

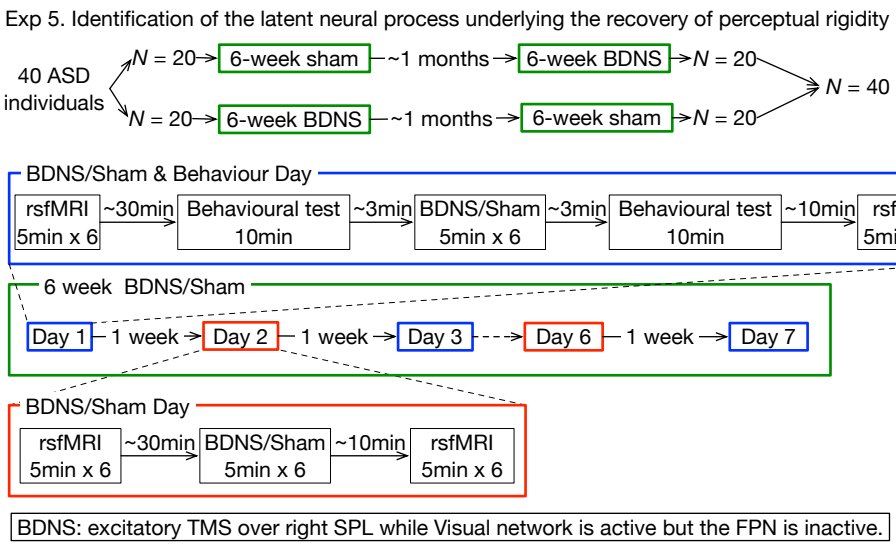

Supplementary Fig. 7. **Design of Experiment 5.** In this additional BDNS experiment, we directly examined the brain-behaviour causality between the FPN-VN coupling and perceptual rigidity.

Supplementary Fig. 8

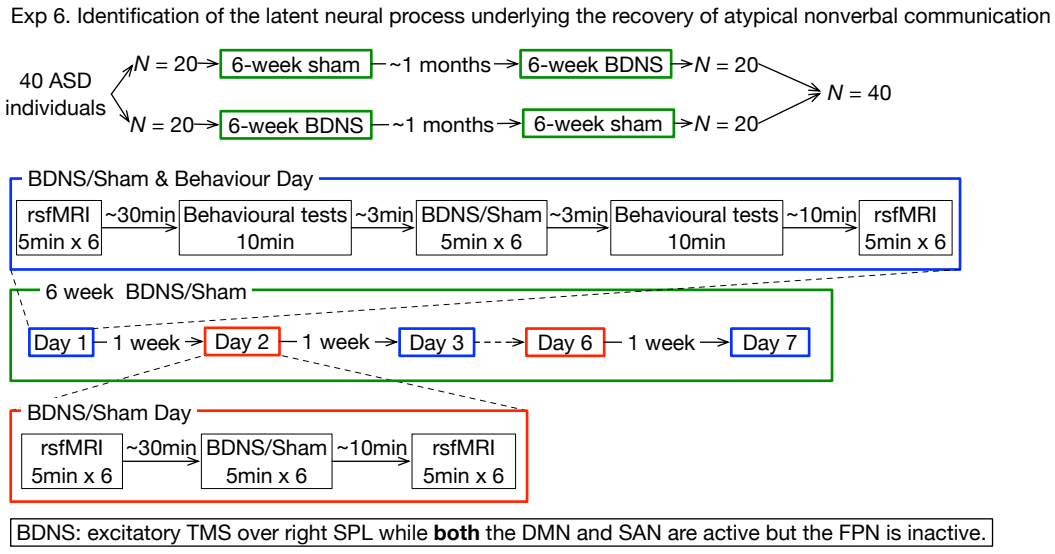

Supplementary Fig. 8. **Design of Experiment 6.** We conducted another six-week BDNS experiment and directly examined the causality between the FPN-DMN-SAN coupling and the atypical nonverbal communication.

Supplementary Fig. 9

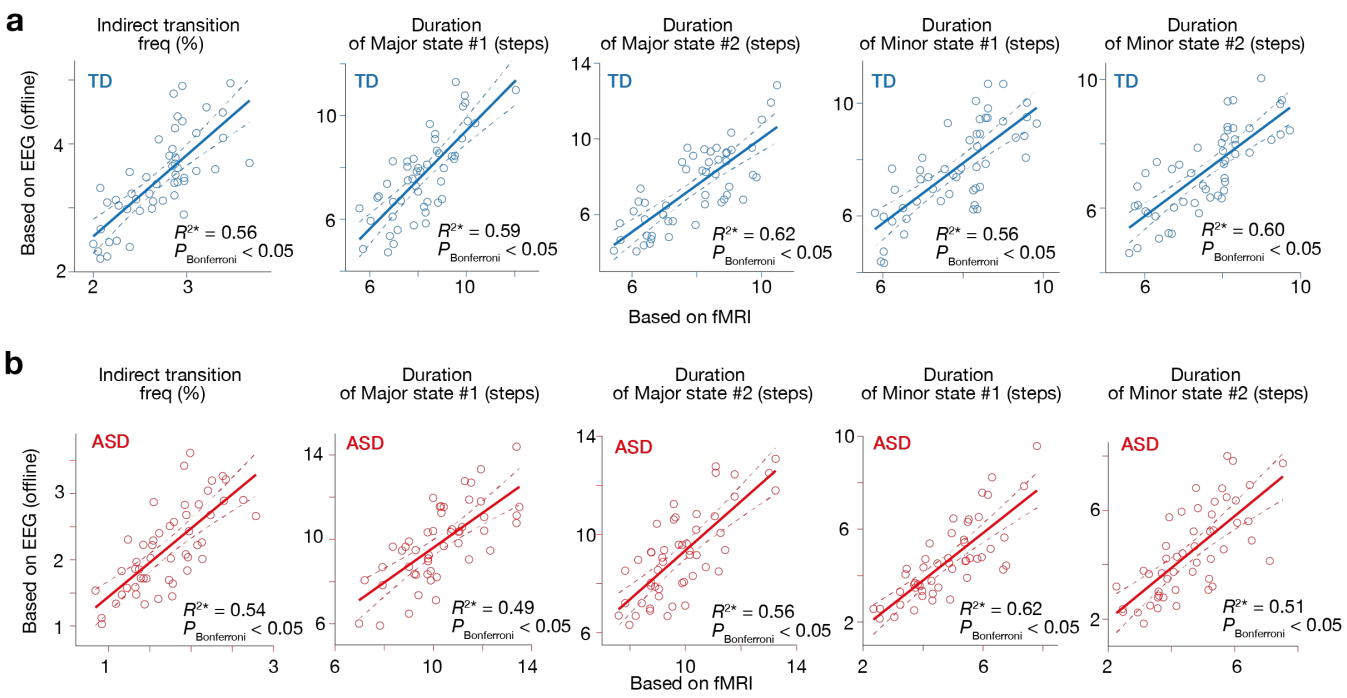

Supplementary Fig. 9. Comparison of brain dynamics based on the offline EEG data with those based on the fMRI data. (a & b) To evaluate the EEG-based brain state tracking, we performed the following two analyses: (i) we first examined whether energy landscape analysis using offline-preprocessed EEG data could identify qualitatively the same brain dynamics as those based on the fMRI data; (ii) we then compared the brain states identified in the offline EEG analysis with those in the online EEG analysis.

Even using the EEG data that were preprocessed in an offline manner, we obtained qualitatively the same energy landscapes in both the TD and ASD groups. The EEG-based energy landscapes had the same four local minima as those seen in the fMRI-based energy landscape analysis (**Figs. 2a and 2l**).

In addition, the brain dynamics based on the energy landscapes using two different types of neural data exhibited significant similarities: the indirect transition frequency, durations of major states #1/#2 and durations of minor states #1/#2 calculated using offline-preprocessed EEG data were significantly associated with those based on fMRI data (R^{2*}>0.49, $P_{Bonferroni}$<0.05).

These observations indicate that the brain dynamics determined in the offline analysis of the EEG data could capture qualitatively the same brain-state trajectories as those observed in the analysis of the fMRI data. In both the TD and ASD groups, we observed significant associations between the EEG-based brain dynamics and fMRI-based ones. The indirect transition frequency, duration of major states #1/#2 and duration of minor states #1/#2 showed significant correlations. Each dot represents each participant.

Supplementary Fig. 10

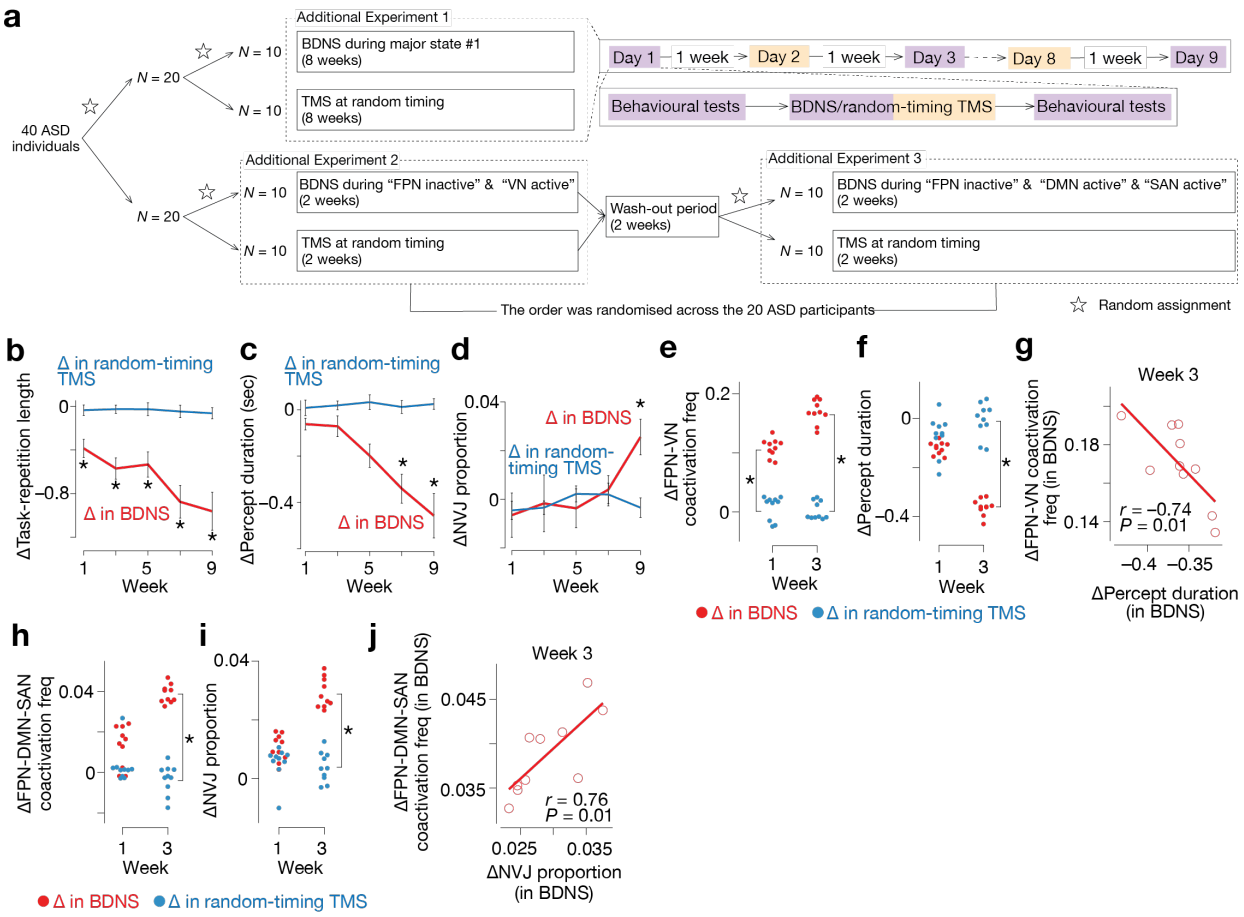

Supplementary Fig. 10. **Results of the three additional experiments: BDNS v random-timing TMS.** To examine the robustness of the original behavioural effects of the BDNS, we performed three additional experiments with active control conditions (here, random-timing TMS condition). **(a)** The three additional experiments employed the same 40 autistic individuals who completed Experiment 4. The participants were randomly split into the following two groups: 20 of them were assigned to Additional Experiment 1, which was designed to examine the robustness of the results of Experiment 4; the other 20 participants underwent Additional Experiments 2 and 3, which were set to validate the reproducibility of the results of Experiments 5 and 6, respectively. **(b-d)** Even against the active control condition, the BDNS over the right SPL during the major state #1 mitigated the cognitive inflexibility, perceptual overstability and atypical nonverbal information processing, which was consistent with the findings of Experiment 4. **(e-g)** Compared to the random-timing TMS condition, the BDNS condition increased the FPN-VN coactivation frequency (Week 1 and 3) and mitigated the percept overstability (Week 3). The neural effect was correlated with the perceptual change. **(h-j)** Compared to the active control, the BDNS condition strengthened the FPN-DMN-SAN coupling and enhanced the utilisation of the nonverbal social information at Week 3. This change in the triad network coupling was correlated with the behavioural effect. *, $P_{Bonferroni} < 0.05$.

Supplementary Tables

Supplementary Table 1. **Demographic data of participants**

	TD	ASD	ADHD v TD
N	50	50	
Age (mean±sem)	23.4±0.3	22.9±0.3	*P* = 0.3
Sex	14 females	11 females	*P* = 0.5
FIQ	119.6±1.6	120.3±1.7	*P* = 0.7
VIQ	119.1±1.7	120.9±2.1	*P* = 0.4
PIQ	116.4±1.4	115.9±1.6	*P* = 0.8
ADOS Social	—	3.6±0.2	—
ADOS Communication	—	7.7±0.2	—
ADOS RRB	—	0.7±0.1	—

FIQ/VIQ/PIQ, Full-scale/Verbal/Performance Intelligence Quotient. ADOS, Autism Diagnostic Observation Schedule.

Supplementary Table 2. **Effect size and necessary sample size**

Cohen's *d*	0.57	0.58	0.59	0.6	0.61	0.62
sample size	42	41	40	39	37	36

Supplementary Methods

1. Participants and ethics

1.1. Sample size

This study recruited 50 high-functioning right-handed adults with autistic spectrum disorder (ASD) and 50 age-/IQ-/sex-/laterality-matched typically developing (TD) individuals (**Supplementary Table 1**). We employed ASD adults here because this study asked the participants to undergo a series of TMS sessions, whose protocol was not allowed for autistic children in Japan.

This sample size was determined based on our previous studies. In one of the studies[1], we measured the cognitive inflexibility in high-functioning ASD adults using the same spontaneous task-switching test as in the current research and reported that the task-repetition length of the autistic individuals was 3.7±0.6 (mean±SD). In the other work[2], we found that the BDNS could increase perceptual stability by approximately 7–7.5%. Given these, we assumed that BDNS could induce behavioural changes with 0.57–0.62 of effect size (Cohen's *d*) and performed power analyses (power = 0.8, α = 0.05). As a result, we found that 36–42 autistic participants were necessary for us to detect such statistically significant behavioural differences (**Supplementary Table 2**).

In addition, we assumed that ~20% of the participants would drop out from the current longitudinal experiments whose lengths were >24 weeks at most and recruited 50 ASD individuals. As for the TD group, we recruited the same number as a control. Note that the seemingly low RRB score was comparable to that seen in high-functioning adults with ASD (FIQ≥85) in ABIDE[3].

1.2. Selection criteria

The participants were diagnosed by a trained psychiatrist according to DSM 5, and the severity of their core symptoms was assessed using ADOS-2 Japanese edition[4] by the psychiatrist and/or a trained psychologist. To reduce the heterogeneity of the participants, this study employed high-functioning ASD adults (Full IQ/Verbal IQ/Practice IQ ≥ 85). The IQ was quantified with the Wechsler Adult Intelligence Scale (third edition, UK). We excluded individuals with any other neuropsychiatric disorders and those taking psychiatric medicines at the time of the experiments.

1.3. Ethics

This study was approved by Institutional Ethics Committees at The University of Tokyo (20-132). The protocols for transcranial magnetic stimulation (TMS) complied with the guidelines issued by the Japanese Society for Clinical Neurophysiology and the International Federation of Clinical Neurophysiology[5]. All the participants provided written informed consent before any experiment and were financially compensated for their participation.

2. Study design

2.1. Overall design

This study consisted of six experiments and one numerical simulation study (**Fig. 1f**).

In Experiment 1, we collected resting-state functional MRI (rsfMRI) data from the 50 participants with ASD and 50 TD individuals. For the following BDNS experiments, we also obtained resting-state EEG (rsEEG) data from the same participants.

We then conducted the numerical simulation study on the neural effects of the brain-state-driven neural stimulation (BDNS) and searched for the candidates for the optimal BDNS protocol that would mitigate the autistic neural rigidity the most.

For the empirical validation of the results of the numerical simulation, we conducted Experiment 2, which consisted of three parts. In Experiment 2-1, we compared the neural effects between three BDNS over three different target brain regions. In Experiment 2-2, we compared the neural effects between four BDNS during four different stimulation timings. In Experiment 2-3, we performed a conventional 30-min repetitive TMS[6,7] as a control condition.

Based on the results of the above experiments and simulation, we then conducted Experiments 3 and 4. In the former experiment, we assessed the neural and behavioural effects of single BDNS, whereas we examined the longitudinal effects in the latter.

In Experiments 5 and 6, we searched for the latent neural processes in which the BDNS-induced mitigation of the neural rigidity transformed into the mitigation of the perceptual rigidity (Experiment 5) and atypical nonverbal communication (Experiment 6) in autism.

In all the experiments employing TMS, the experimenters knew the experimental conditions in prior, whereas the participants were not informed about which condition (i.e., TMS or control) they were about to undergo.

2.2. Experiment 1

We collected the rsfMRI and rsEEG data from all the 50 TD and 50 ASD individuals (**Supplementary Fig. 1**). We used the rsfMRI data, which were obtained in six 5-min runs, to (i) identify the individual brain state dynamics at the baseline for the following simulation and experiments and (ii) examine the associations between the autistic neural rigidity and its atypical behaviours. The following 20-min rsEEG data were used to optimise the preprocessing protocols of the EEG data so that we could obtain qualitatively the same brain state dynamics as those seen in the analysis using the rsfMRI data. In this EEG recording, we also mapped the locations of the EEG electrodes onto the individual brain using a stereoscopic neuro-navigation system (Brainsight Neuronavigation, Rogue Research, UK).

2.3. Numerical simulation

Based on the individual energy landscape structure calculated in Experiment 1, we numerically searched for the candidates for the optimal stimulation protocol. This analysis was performed only for the autistic individuals.

First, in a brute-force manner, we identified which of the nine brain networks should be activated/inhibited by the BDNS. We performed such network-wise simulations because, as in our previous study[8], the energy landscape analysis was conducted using the nine average neural activities for the following nine networks[9]: default mode network (DMN, 59 regions), frontoparietal network (FPN, 25 regions), salience network (SAN, 18 regions), dorsal attention network (DAN, 11 regions), ventral attention network (VAN, 9 regions), cingulo-opercular network (CON, 14 regions), somatosensory network (SMN, 34 regions), auditory network (AN, 13 regions) and visual network (VN, 31 regions).

Second, we specified which brain region of the identified brain network—here, FPN—should be stimulated by calculating the average of the within-network functional connectivity for each FPN region.

The step-by-step procedures of this simulation are described in **Section 8**.

2.4. Experiment 2-1

The numerical study identified three candidates for the stimulation target. Then, we narrowed down them to one region by conducting three types of BDNS experiment employing 48 individuals who were randomly chosen from the 50 ASD participants (**Supplementary Fig. 2**).

The 48 participants were randomly assigned to one of the three experiments and underwent one BDNS and one sham session over one of the three target brain regions. The order of the BDNS and sham conditions were randomly determined across participants, and the two types of experiments were performed at an approximately two-week interval.

In the BDNS session, we administered an excitatory TMS over one of the three target regions while the participants' brains were staying in the major state #1. The BDNS conditions (i.e., excitatory TMS during the major state #1) were determined based on the numerical study.

The settings of the sham session were the same as those of the BDNS session except that the TMS coil made the same sound as in the BDNS session but did not induce any electro-magnetic change in the brain.

We evaluated the effects on the neural rigidity by calculating the alternation of the indirect transition frequency between the BDNS and sham sessions as follows:

$$\text{Neural Effect} = ([\text{Indirect transition freq}]_{\text{Post-BDNS}} - [\text{Indirect transition freq}]_{\text{Pre-BDNS}}) - ([\text{Indirect transition freq}]_{\text{Post-Sham}} - [\text{Indirect transition freq}]_{\text{Pre-Sham}}). \quad \textbf{Equation 1}$$

2.5. Experiment 2-2

Experiment 2-1 allowed us to identify a specific brain region—here, the right superior parietal lobule (SPL)—over which the BDNS during the major state #1 induced the largest neural effect.

In Experiment 2-2, we empirically examined whether such a stimulation timing (i.e., during major state #1) was the most efficient (**Supplementary Fig. 3**). Technically, we first randomly selected 48 individuals from the 50 autistic participants and assigned them to one of the following four conditions randomly. In the four conditions, we administered an excitatory TMS over the right SPL when the participants' brains were staying at four different brain states: major state #1, major state #2, minor state #1 and minor state #2.

The effects of the four different types of BDNS were assessed by comparing the changes in the indirect transition frequency between the BDNS and sham conditions (see **Equation 1**). The order of the BDNS and sham sessions was randomised across the participants.

2.6. Experiment 2-3

For comparison, we investigated the neural effects of the conventional 30-min excitatory receptive TMS (rTMS) over the target brain region we identified in Experiment 2-1(i.e., right SPL; **Supplementary Fig. 4**). This experiment employed 30 individuals who were randomly chosen from the 50 ASD participants, and the rTMS protocol was the same as that used in our previous studies[6,7]. We evaluated the effects of this conventional rTMS by comparing the change in the indirect transition frequency between the rTMS and sham conditions (see **Equation 1**). The order of the rTMS and sham conditions was randomly determined across participants. The details of the rTMS are described in **Section 7**.

2.7. Experiment 3

Based on the optimised BDNS protocol, we first examined the behavioural effects of a single BDNS (**Supplementary Fig. 5**). All the 50 autistic individuals participated in this experiment. After rsfMRI scanning (six 5-min runs), the participants underwent the three behavioural tests—spontaneous task-switching test (**Section 3.1),** bistable perception test (**Section 3.2**) and friend-or-foe test (**Section 3.3**)—in a pseudo-random order. The neural and behavioural effects were calculated based on the **Equation 1**.

2.8. Experiment 4

We then examined the longitudinal neural and behavioural effects of the BDNS in high-functioning autistic adults (**Supplementary Fig. 6**). To this aim, we adopted a sham-controlled, cross-over design, which consisted of two 12-week BDNS/sham periods with an approximately two-month washout interval.

In the 12-week period, the participants underwent 13 weekly BDNS/sham sessions in total. To track the neural effects, we also collected the rsfMRI data from them every week. As to the behavioural effects, the participants were asked to take the three behavioural tests every two weeks. We did not perform the behavioural tests every week to (1) reduce the psychological burden for the participants and (2) decrease the possibility that the participants became overly accustomed to the psychological tests.

None of the 50 ASD participants reported adverse effects even three months after this longitudinal experiment; however, 10 of them did not complete the experiment due to its length.

2.9. Experiment 5

We conducted Experiment 5 to investigate neural mechanisms by which the mitigation of the perceptual rigidity was slower than that of the cognitive inflexibility. Given the finding that the alleviation of the perceptual rigidity was correlated with the coactivation frequency between the frontoparietal network (FPN) and visual network (VN), we examined whether the direct intervention to enhance the FPN-VN coactivation could mitigate the perceptual rigidity more quickly compared to the original BDNS protocol. Technically, we administered the same magnitude of excitatory TMS over the same right SPL while the VN was active but the FPN was inactive. Note that the FPN-VN coactivation frequency was calculated through direct counting of the binarised network-wise fMRI signals obtained in Experiment 1. That is, we estimated how frequently the brain activity pattern with “FPN active” and “VN active” was seen in the individual time-series fMRI data.

The design of this experiment is essentially the same as that of Experiment 4 (Section 2.8) except for the length of each BDNS/sham period. In this experiment, we set it at six weeks since the behavioural effects were supposed to emerge more rapidly. Also, this experiment focused on the perceptual rigidity and, thus, did not examine the cognitive rigidity or atypical nonverbal communication in autism.

The 40 autistic individuals, who completed Experiment 4, participated in this experiment. No adverse effect was reported.

2.10. Experiment 6

We performed Experiment 6 to investigate the neural processes in which the mitigation of the neural rigidity mitigated the atypical nonverbal communication in autism.

Based on previous findings, we hypothesised that the enhanced functional coupling between the FPN, default mode network (DMN) and salience network (SAN) would be the key process for the alleviation of the autistic social cognition.

To test this, we first assessed the FPN-DMN-SAN coactivation frequency in the ASD individuals and correlations between the network coupling strength and autistic nonverbal information processing traits (i.e., NVJ proportion). Note that the FPN-DMN-SAN coactivation frequency was calculated through direct counting of the binarised network-wise fMRI signals obtained in Experiment 1. That is, we estimated how frequently the brain activity pattern with "FPN active", "DMN active" and "SAN active" was observed in the individual time-series fMRI data.

Then, we directly examined the association between the triad network coupling and the alleviation of autistic nonverbal information processing by conducting a longitudinal experiment (**Supplementary Fig. 8**) with the same design and participants as in Experiment 5 (**Section 13**). The experiment focused on the effects on the atypical nonverbal communication and, thus, the participants underwent only the friend-or-foe test.

To examine the effects of enhancing the FPN-DMN-SAN coupling, we administered the same magnitude of excitatory TMS over the same SPL while both the DMN and SAN were simultaneously active but the FPN was inactive.

Here, we assessed (i) the indirect transition frequency, (ii) the FPN-DMN-SAN coactivation frequency and (iii) the proportion of the nonverbal information-based judgements in the friend-or-foe test.

3. Behavioural tests

This study adopted three psychology tests to evaluate three different autistic traits: spontaneous task-switching test to evaluate the cognitive inflexibility, bistable perception test to assess the perceptual rigidity and friend-or-foe test to quantify the atypical nonverbal communication style in autism.

3.1. Cognitive inflexibility: spontaneous task-switching test

3.1.1. Paradigm

This psychology test was built based on previous studies[10,11], and its current setting was the same as those in our prior work[1]. We adopted this test to assess autistic cognitive inflexibility. In fact, conventional instruction-based task-switching tests, such as the Wisconsin Card Sorting Test, often show relatively low sensitivity to the autistic cognitive rigidity[11,12], whereas multiple behavioural studies demonstrated that the spontaneous task-switching test could reveal this ASD-specific behavioural tendency even when the autistic individuals had normal or above-normal intelligence[1,10,11].

The participants were presented with visual stimuli that had four figures with different shapes and brightness; then, we asked them to perform a 'shape task' or a 'brightness task'.

In the shape task, the participants were asked to identify a specific shape (e.g., a circle), whereas they were asked to identify the brightest (or darkest) figure in the brightness task.

They were asked to press one of four buttons to indicate their choice for each task as accurately and quickly as possible. When the participants did not press any of the buttons in 3 sec, the trial automatically ended, and the next trial started.

The participants were informed that they could freely choose which task they would conduct for each trial. As in previous studies[1,10,11], we told them as follows:

> "*You have to choose which task to perform on each trial. Ideally, you should perform each task randomly but on about half of the trials. Sometimes you will repeat the same task and sometimes you will switch from one to another. We don't want you to count the number of times you've done each task or alternate strictly between tasks to make it sure that you do each one half the time. Just try to do them randomly.*"

3.1.2. Analysis

Based on the records of the chosen figures, we inferred which task the participants chose for each trial and labelled every trial into a shape or brightness trial. Note that the participants chose a figure that could not be classified into either a shape or brightness task sufficiently rarely (such unclassifiable trials, ≤1.2% of the entire trials). Therefore, we excluded such unclassifiable trials and counted how many times the participants repeated the same type of task.

Based on our previous work[1], the task-repetition length was used as a metric for autistic cognitive inflexibility here.

On all the behavioural experiment days, the participants completed practice of this spontaneous task-switching test until they could respond correctly (≥95% of accuracy) and quickly (reaction time ≤2 sec). Afterwards, the participants underwent this test four times (3 min for one run).

3.2. Perceptual rigidity: bistable perception test

3.2.1. Paradigm

The perceptual rigidity was assessed using the same bistable visual perception paradigm as that used in our previous studies[1,2,13].

This bistable perception was induced by a structure-from-motion (SFM) stimulus, a sphere consisting of 200 sinusoidally moving white dots in a black background (angular velocity, 120°/sec) with a fixation cross (0.1° × 0.1°) at the centre of the 27-inch LCD monitor (BenQ PD2710, resolution: 2560×1440). The stimulus presentation and response recording were conducted with PsychToolbox 3 in MATLAB (MathWorks, Inc).

The participants were presented with this stimulus for 90 sec for each run with their chins on a chin rest. They were asked to press one of the three buttons according to their visual perception: one for upward rotation, another for downward rotation, and the other for unsure or mixture perception. After training, the participants repeated this run five times.

3.2.2. Analysis

All the 50 ASD and 50 TD participants experienced the mixture perception rarely (1.2±0.3% of all stimulus presentation times, mean±sd); thus, we excluded such time periods from the following behavioural analyses.

We calculated the duration of such clear perception and estimated the median of the duration. We adopted this metric because previous studies reported atypical prolongation of the percept duration in autism[1,14–16], and the time length can be seen as an index for autistic perceptual rigidity.

3.3. Atypical nonverbal communication: friend-or-foe test

3.3.1. Paradigm

This test was developed in our previous studies to evaluate socio-communicational symptoms seen in high-functioning autistic adults[17–19]. Here, we used the same stimuli and settings as in the prior works[17,19] that successfully detected oxytocin's beneficial effects on the core symptom of ASD with this psychological test.

In this social cognition test, we presented the participants with 80 short monochrome videos (1.5sec). In each video, one of 20 professional actors spoke an emotional word (verbal information) with a specific emotional facial expression and voice prosody (nonverbal information). Note that the facial expression and voice prosody in one video indicated the same emotional direction.

We prepared four types of videos, two with congruent stimulus and two with incongruent stimulus. The 40 congruent stimuli consisted of 20 videos with 'positive nonverbal and verbal information' and 20 other videos with 'negative nonverbal and verbal information'. The 40 incongruent stimuli comprised 20 videos with positive nonverbal information and negative verbal information—which are similar to jokes—and 20 other videos with negative nonverbal information and positive verbal information—which are similar to ironies—.

In a 2-sec period right after each video, the participants were asked to judge whether the actor appeared to be a friend or foe to them. After sufficient training sessions with different stimuli, the participants were pseudo-randomly presented with these movies and made friend-or-foe judgements.

3.3.2. Analysis

As in our previous studies[17–19], we focused on the responses to the incongruent stimuli since they highlight the autistic social cognition. First, we classified the responses into 'nonverbal information-based judgment (NVJ)' and 'verbal information-based judgement (VJ)'. That is, if the participants regarded as foes the actors who spoke a positive word in a negative facial expression and voice prosody, such decisions were classified as NVJs. When the actors who spoke a negative word with positive facial and voice expressions were taken as foes, the decisions were classified as VJs.

Since high-functioning autistic adults are known to make significantly fewer NVJs compared to TD adults[18], we tracked the proportion of the NVJs to evaluate how the atypical social cognition in autism was mitigated in the longitudinal BDNS.

4. MRI recording and analysis

4.1. Recording

In this study, we recorded structural and resting-state functional MRI using a 3.0T MRI scanner (Trio, Siemens Medical Systems) with the 32-channel head coil at the International Research Center for Neurointelligence (WPI-IRCN) at The University of Tokyo. T1-weighted structure images were obtained at 1mm-cubic resolution (TR 2.25sec, TE 4.52msec, Flip angle 9 degrees). Resting-state functional images were recorded using an echo planar imaging (EPI) sequence (TR 0.8sec, TE 37ms, Flip angle 52 degrees, 72 slices, spatial resolution 2×2×2mm, multi-band acceleration factor 8). Phase image and magnitude images were also obtained for a fieldmap.

During the recording of the functional images, the participants were asked to open their eyes and watch a fixation cross at the centre of the screen without thinking about specific issues.

4.2. Preprocessing

The EPI data were preprocessed with SPM12 (www.fil.ucl.ac.uk/spm) in the same way as in our previous studies using the energy landscape analysis for rsfMRI data[8,20]. First, the first five images were discarded, and the images underwent realignment, unwarping, slice timing correction, normalisation to the standard template (ICBM 152) and spatial smoothing (Gaussian kernel with 8mm of full-width at half maximum). Then, we removed the effects of head motion (X, Y, Z, pitch, roll and yaw), white matter signals, cerebrospinal fluid signals and global signals before performing band-pass temporal filtering (0.01–0.1Hz). No significant difference was found in any of the six parameters for the head motion between the ASD and TD individuals ($P > 0.6$). The framewise displacement showed no significant difference between the ASD and TD groups, either ($P > 0.4$).

4.3. Energy landscape analysis

We performed the energy landscape analysis in essentially the same manner as in our previous studies[2,8,13,20]. Note that this study basically performed the analysis at an individual level; we conducted the group-level analysis only when we needed to present the representative brain state dynamics and energy landscape structure.

Also, we have to note that the energy landscape analysis was performed based on network-wise rsfMRI signals rather than region-wise ones, mainly due to the data limitation. To obtain accurate results from the energy landscape analysis of time-series data recorded from N nodes, we have to collect data with more than 2^N time points. Therefore, it was practically impossible to conduct the energy landscape analysis without summarising neural signals recorded from a whole brain. For example, if we adopted a widely used brain parcellation system[9] developed by Power et al, a whole brain was divided into approximately 250 regions. Thus, region-wise energy landscape analysis would require us to record rsfMRI data with more than 2^{250} ($>10^{77}$) time points. To circumvent this technical difficulty, we summarised the ~250 regions into the nine brain networks, which only required 2^9-timepoint rsfMRI data at least. In fact, this network-wise energy landscape analysis worked well in previous studies[8,20].

4.3.1. Network-wise rsfMRI signals and binarization

By applying this data-driven analysis to the rsfMRI data, we investigated network-based neural dynamics.

First, based on a widely used brain parcellation system[9], we divided the cerebral cortex into the following nine functionally distinct networks: the default mode network (DMN, 59

regions), frontoparietal network (FPN, 25 regions), salience network (SAN, 18 regions), dorsal attention network (DAN, 11 regions), ventral attention network (VAN, 9 regions), cingulo-opercular network (CON, 14 regions), somatosensory network (SMN, 34 regions), auditory network (AN, 13 regions) and visual network (VN, 31 regions). We adopted this segmentation system because our previous studies using basically the same parcellation system succeeded in capturing brain state dynamics specific to ASD[8,20], ADHD[20] and ASD+ADHD comorbidity[20].

Technically, we extracted time-series rsfMRI data from each region of interest, which was defined as a 4-mm-radius sphere around the pre-determined MNI centre coordinate, and assigned to the corresponding network based on the parcellation system[9]. Next, we calculated the average rsfMRI signal for each network at each time point for each participant. That is, we normalised the network rsfMRI signal by the number of the brain regions in each network, which reduced the confounding effects of the network size on the following analysis. We then binarised the network activities using the whole-brain average fMRI signal at each time point as a threshold (+1 for active and –1 for inactive). That is, the threshold varied between different time points, and using such a time-point-specific threshold, we repeated this binarisation throughout the time-series data.

The binarisation procedure balanced the numbers of active and inactive states and should improve the accuracy of the following analysis[21], which was also face-validated in our previous work[2,8,20,22]. After this procedure, an activity pattern of the nine networks at time point t was described as $V^t = [\sigma_1^t, \sigma_2^t, \ldots, \sigma_N^t]$, where σ_i^t represents a binary activity of network i at time t (i.e., $\sigma_i^t = +1 \text{ or } -1$) and N denotes the number of the networks (here, $N = 9$).

4.3.2. Fitting of a pairwise maximum entropy model

Second, we fitted a pairwise maximum entropy model (MEM) to the binary data.

We chose a pairwise MEM since it is among the simplest models to describe collective network dynamics that occur on interactions between multiple nodes. In fact, a pairwise MEM is built upon two types of parameters: h_i and J_{ij}. The h_i denotes the basal activity of node i (here, brain network i), and J_{ij} represents a pairwise interaction between node i and node j. Neurobiologically, this model simply assumes that different nodes have different intrinsic activity h_i and different pairs of nodes have different coupling strengths J_{ij}.

In addition, as to J_{ij}, this assumption was confirmed, at least, in rsfMRI data. A previous rsfMRI human study reported the similarity between the J_{ij} and conventional functional connectivity (FC), which is based on Pearson's correlation coefficients[21]. Even in this study, the rsfMRI data obtained in Experiment 1 showed significant correlations between J_{ij} and FC both in the ASD and TD groups ($r_{34} = 0.38$, $P = 0.022$ for ASD; $r_{34} = 0.42$, $P = 0.011$ for TD). That is, a pairwise MEM could be regarded as a simple and biologically plausible model to describe collective neural dynamics.

Moreover, a line of previous studies demonstrated that a pairwise MEM is well fitted to various types of collective neural activity, including spike recording[23–26], local field potential[26], fMRI signals[13,21,27,28] and EEG data[2]. Furthermore, some of these studies showed that, based on the pairwise MEM, we can infer attractor-based brain

dynamics[2,8,13,27,28]. Given these, we adopted a pairwise MEM to invesitage the collective brain network.

The two types of parameters, h_i and J_{ij}, were determined so that the average of the model-based network activity $\langle\sigma_i\rangle_{\mathrm{m}}$ and the average of the model-based pairwise interactions $\langle\sigma_i\sigma_j\rangle_{\mathrm{m}}$ are close to the average of the empirical network activity $\langle\sigma_i\rangle$ and the average of the empirical pairwise interaction $\langle\sigma_i\sigma_j\rangle$, respectively.

The $\langle\sigma_i\rangle_{\mathrm{m}}$ was defined as

$$\langle\sigma_i\rangle_{\mathrm{m}} = \Sigma_{\ell=1}^{2^N}\sigma_i(V_\ell)P(V_\ell),$$

and the $\langle\sigma_i\sigma_j\rangle_{\mathrm{m}}$ was defined as

$$\langle\sigma_i\sigma_j\rangle_{\mathrm{m}} = \Sigma_{\ell=1}^{2^N}\sigma_i(V_\ell)\sigma_j(V_\ell)P(V_\ell),$$

where $\sigma_i(V_k)$ is the activity of network i in the activity pattern V_k and $P(V_k)$ is the appearance probability of the neural activity pattern V_k. The $P(V_k)$ is given as

$$P(V_k) = e^{-E(V_k)}/\Sigma_{\ell=1}^{2^N}e^{-E(V_\ell)},$$

where

$$E(V_k) = -\Sigma_{i=1}^{N}h_i\sigma_i(V_k) - (1/2)\Sigma_{i=1}^{N}\Sigma_{j=1}^{N}J_{ij}\sigma_i(V_k)\sigma_j(V_k).$$

$E(V_k)$ represents a hypothetical energy value assigned to the network activity pattern, V_k. Conceptually, V_k with lower $E(V_k)$ is likely to be more stable and exhibit a larger appearance probability. The following energy landscape is built based on these energy values.

Based on these definitions, we adjusted h_i and J_{ij} until the $\langle\sigma_i\rangle_{\mathrm{m}}$ and $\langle\sigma_i\sigma_j\rangle_{\mathrm{m}}$ were approximately equal to the $\langle\sigma_i\rangle$ and $\langle\sigma_i\sigma_j\rangle$ with a gradient ascent algorithm. The iteration scheme is given by

$$h_i^{\mathrm{new}} = h_i^{\mathrm{old}} + \alpha\cdot\log(\langle\sigma_i\rangle/\langle\sigma_i\rangle_{\mathrm{m}}) \text{ and}$$
$$J_{ij}^{\mathrm{new}} = J_{ij}^{\mathrm{old}} + \alpha\cdot\log\left(\langle\sigma_i\sigma_j\rangle/\langle\sigma_i\sigma_j\rangle_{\mathrm{m}}\right),$$

where α is the learning rate and set at 0.1. During this iteration, we calculated the relative gaps between the model and empirical data as follows:

$$ErrorMEM = \max(\max_i|(\langle\sigma_i\rangle_{\mathrm{m}} - \langle\sigma_i\rangle)/\langle\sigma_i\rangle|, \max_i\left|\left(\langle\sigma_i\sigma_j\rangle_{\mathrm{m}} - \langle\sigma_i\sigma_j\rangle\right)/\langle\sigma_i\sigma_j\rangle\right|).$$

We continued this adjustment until *ErrorMEM* was smaller than 10^{-10} (see ***Extended Data Fig. 2*** for an example of this adjustment of the rsfMRI data obtained from Participant #1 in the ASD group in Experiment 1).

The accuracy of this fitting, r_D, was assessed based on a proportion of Kullback-Leibler (KL) divergence in this 2nd-order model (D_2) to that in the 1st-order model (D_1)[2,8,13,20,21] as follows:

$$r_D = (D_1 - D_2)/D_1.$$

Here, the 1st and 2nd-order models indicate independent and pairwise MEM, respectively. Whereas the pairwise MEM, which we adopted here, assumes both the basal activity (h_i) and pairwise interactions (J_{ij}), the independent MEM did not assume the pairwise interaction and determined the h_i under the condition that $J_{ij} = 0$. That is, for the independent MEM, $\langle \sigma_i \sigma_j \rangle_{\mathrm{m}}$ equals $\langle \sigma_i \rangle_{\mathrm{m}} \langle \sigma_j \rangle_{\mathrm{m}}$.

4.3.3. Energy landscape structure

Based on the h_i and J_{ij}, we built an energy landscape for each individual. The landscape was defined as a graph of brain activity patterns V_k ($k = 1, 2, \ldots, 2^N$), in which two activity patterns were regarded as adjacent if and only if their difference was seen at only one network activity. That is, V_m and V_n are adjacent to each other if and only if the Hamming distance between the two vectors is 1. For example, a network activity [1, 1, 1, 1, 1, 1, 1, 1, 1] is adjacent to [–1, 1, 1, 1, 1, 1, 1, 1, 1] but not adjacent to [–1, –1, 1, 1, 1, 1, 1, 1, 1] because the former one has only one difference but the latter has two.

We first searched for local energy minima, whose energy values were smaller than those of all the N adjacent patterns. We then examined the hierarchical structures between the local minima by building a disconnectivity graph as follows[2,8,13,20]:

(i) We prepared a hypercube graph, in which each node (i.e., each brain activity pattern) was adjacent to the N neighbouring nodes.

(ii) We set a threshold energy level, $E_{\mathrm{threshold}}$, at the largest energy value among the 2^N nodes.

(iii) We then removed the nodes whose energy values $E(V_k)$ were greater than $E_{\mathrm{threshold}}$.

(iv) We examined whether each pair of local minima was still connected by a path in the slightly disconnected graph.

(v) We repeated steps (iii) and (iv) after changing $E_{\mathrm{threshold}}$ down to the next largest energy value

(vi) We stopped these procedures when all the remaining local minima were isolated.

(vii) Based on the obtained results, we built a hierarchical tree—disconnectivity graph—whose leaves (i.e., terminal nodes down in the tree) represented the local minima and internal nodes indicated the branching points of different local minima.

4.3.4. Classification to basins

Based on this individual disconnectivity graph, we classified all the brain activity patterns V_k ($k = 1, 2, \ldots, 2^N$) into one of the basins with a corresponding local minimum at their bottoms.

First, we picked up a brain activity pattern V_i from the 2^N patterns. If any of its neighbour patterns had a smaller energy value than V_i, we moved to such a brain activity pattern. Otherwise, we did not move because the V_i was a local minimum. We repeated this procedure for all the V_i until we reached any of the local minima. The initial V_i was then classified into a member of the basin of the local minimum that we finally reached. This procedure allowed us to classify all the brain activity patterns on the energy landscape—except for nodes on the saddles—into any of the basins.

4.3.5. Energy barriers

We then calculated the heights of the energy barriers between the local minima (e.g., local minima ℓ and m).

This energy barrier height was defined in the procedure of building the disconnectivity graph as follows. When we built the disconnectivity graph, we lowered the threshold energy level $E_{\text{threshold}}$. During this process, we searched for the lowest $E_{\text{threshold}}$ at which the two local minima ℓ and m were still connected. Then, the height of the energy barrier from local min ℓ to m was defined as the gap between the $E_{\text{threshold}}$ and the energy value for the local min ℓ. The energy barrier height from local min m to ℓ was defined as the difference between the $E_{\text{threshold}}$ and the energy value for the local min m.

Then, as in our previous work[2,8,13], we summarised the local minima. If the energy barrier height from the local min ℓ to m was lower than a threshold and if the energy value of the local min ℓ was larger than that of local min m, the local min ℓ and its basin were merged into the basin of the local min m. The energy barrier threshold for this summarisation was set at the longest branch length seen in a dysconnectivity graph that was generated from randomised surrogate data.

Through this coarse-graining procedure, we defined the parsimonious number of brain states and calculated structural indices of the energy landscapes (i.e., the height of the energy barrier). Also, this summarisation allowed us to classify all the nodes (i.e., brain activity patterns) on the energy landscape into any of such brain states for each participant.

These merged basins were described as 'brain states', and we calculated mean neural activity patterns for each brain state by averaging the binary brain activity patterns belonging to each brain state. In a group analysis, we also compared such a mean brain activity pattern for each brain state between the TD and ASD groups by estimating Pearson's correlation coefficient between the group-specific brain activity patterns.

4.3.6. Random walk simulation

Using the information on the energy landscape structure and brain state classification, we investigated the brain state dynamics by a random-walk simulation, which was based on a Markov chain Monte Carlo method with the Metropolis-Hastings algorithm[29,30].

In this simulation, a brain activity pattern V_i was allowed to move only to a neighbouring pattern V_j. Technically, we first randomly chose one of such neighbouring patterns and then determined whether a movement to the pattern occurred or not at the probability $P_{ij} = \min\left[1, e^{E(V_i)-E(V_j)}\right]$. That is, when V_i was more unstable than V_j (i.e., $E(V_i) > E(V_j)$), the brain activity pattern always moved from V_i to V_j. In the meantime, this probability setting left some room for moving to V_j even if V_i was more stable than V_j (i.e., $E(V_i) < E(V_j)$), which prevented the brain activity pattern from being stuck in a local minimum forever.

For each individual, we repeated this random walk 10^5 steps with a randomly chosen initial pattern and obtained a trajectory of the brain activity pattern such as $[V^1, V^2, \ldots, V^{10^5}]$. After discarding the first 100 steps to reduce the effects of the initial condition, we classified all the V^t into either of the brain states and converted $[V^{101}, V^{102}, \ldots, V^{10^5}]$ to, for example, [State #1, State #3, State #2, …].

Next, we counted how long each brain state continued in the trajectory (dwelling time) and how often one brain state transited to another state (transition frequency).

These indices based on the random-walk simulation were empirically validated: for each participant, we directly converted its binary time-series data into a brain state trajectory and counted the dwelling time of each brain state and transition frequency between specific brain states.

5. EEG recording and analysis

This study had two types of EEG signal processing: offline analysis for the preparation of BDNS and online analysis during the BDNS, both of which were performed in practically the same manner as in our previous BDNS study[2].

5.1. Recording

We recorded EEG signals using an *eego mylab system* with 256 TMS-compatible Ag/AgCl ring electrodes (ANT Neuro, the Netherlands).

For each participant, we located all the EEG electrodes on individual structural MRI brain images using a stereoscopic neuro-navigation system (Brainsight Neuronavigation, Rogue Research, UK). This localisation for all the electrodes was conducted on the first day of Experiments 1, 3, 5 and 6. On the other days, we measured the locations of the five representative electrodes (Cz, Fpz, Pz, T7 and T8) with the neuro-navigation system. In all the experiment days, we adjusted the location of the EEG cap so that, at least, the locations of the five representative electrodes were practically the same as those measured on the first day of Experiment 1.

We then confirmed that all the electrodes had <5kΩ of impedance and recorded the EEG signals. In a 256-channel amplifier (eego mylab system, ANT Neuro, the Netherlands), the signals underwent low-pass filtering (cut-off frequency: 1.25kHz) and were down-sampled to 3kHz at almost simultaneously (latency <5ms).

Using these settings, we recorded EEG data in six 5-min runs, during which the participants were asked to stare at a fixation cross mark at the centre of the monitor in front of them.

5.2. Offline analysis

To prepare for the BDNS experiments, we applied energy landscape analysis to EEG data in an offline manner.

5.2.1. Preprocessing

We conducted an offline conventional preprocessing[2,31] to the EEG data with MATLAB (MathWorks, US) and EEGLAB[32].

First, we referenced the EEG data to the average across all the electrodes, down-sampled to 300Hz and underwent a temporal filter (1–80Hz). We then performed an independent component analysis (ICA), which was based on short-time Fourier transforms and complex-valued version of FastICA with a robust measure of non-Gaussianity[33], to reduce artefacts induced by cardio-ballistic movements, eye blinks, eye movements and muscle activity.

Next, epochs were marked when the mean global field power was overly large (> 5SD of mean power across the entire recording) and excluded in all the following main analyses. We then filtered the data to delta (1–4Hz), theta (4-8Hz), alpha (8–13Hz), beta (13–30Hz) and gamma (30–80Hz) bands and estimated a Hilbert envelope amplitude for the gamma-band signal[2,31,34].

As in our previous BDNS work[2], this study defined a neural signal for each electrode using the Hilbert envelope amplitude for the gamma band since the gamma-band signal dynamics were known to be correlated with fMRI signals[31,34]. Finally, we removed autocorrelation and estimated a Hjorth signal for each electrode[35].

5.2.2. Classification of electrodes

We then classified the electrodes into one of the nine brain networks based on the localisations of the EEG electrodes onto the cerebral cortex of each participant, which was conducted in Experiment 1 using a stereoscopic neuro-navigation system (Brainsight Neuronavigation, Rogue Research, UK). Technically, we first searched for the region of interest (ROI) in the brain parcellation system[9] that was the nearest to the EEG electrode coordinate. If the distance between the nearest ROI and EEG electrode was less than 4mm, we assigned the EEG electrode to the network to which the ROI also belonged. Otherwise, we excluded the signal of the electrode in the following analysis.

Next, for each network, we calculated the mean network activity by averaging the Hjorth signals of the electrodes belonging to the network.

5.2.3. Energy landscape analysis

Using this network-wise EEG dataset, we conducted the energy landscape analysis. For each participant, the network-wise EEG signals were binarised using the temporal average of the signals as the thresholds[2]. After these operations, a neural activity pattern of the nine brain networks at time t was described such as $V^t = [\sigma_1^t, \sigma_2^t, \dots, \sigma_N^t]$, where σ_i^t represents a binary activity of network$_i$ at time t (i.e., $\sigma_i^t = +1 \text{ or } -1$). N denotes the number of the network (here, $N = 9$). The rest of the energy landscape analysis was exactly the same as that performed for the rsfMRI data (**Section 4.3**).

Using the results of this EEG-based energy landscape analysis, we compared the local minima and transition frequency between the EEG-based and rsfMRI-based energy landscape analysis.

Then, after confirming the similarity between the EEG-based and rsfMRI-based energy landscape analysis (**Supplementary Results**), we summarised the classification information that told us which brain state was assigned to each binary network activity vector. This information would be used in the following online EEG analysis (**Section 5.3.5**).

5.2.4. Preparation for evaluation of online EEG analysis

In parallel, we prepared two types of time-series dataset, which would be used in the comparison of the results based on the offline analysis with those based on the online EEG analysis (**Section 5.3**). Technically, as in our previous study[2], we applied temporal smoothing to the EEG signals that were preprocessed in the offline manner because the online analysis adopted such temporal smoothing.

5.2.4.1. Temporal smoothing of brain state vector

First, using the results of the energy landscape analysis, we applied this temporal smoothing to the time-series vector of the brain states (e.g., [State #1, State #3, State #2, …]). That is, based on a sliding window manner (window length = 10 msec), we calculated the appearance frequency for each brain state in the 10-msec time window and assigned the appearance frequency value to each centre time point in the window as the 'representative appearance frequency' for each brain state. Next, we applied a Gaussian smoothing filter (FWHM = 10msec) to such representative appearance frequency curves. We then assigned the most frequent brain state with the highest representative appearance frequency as the brain state at the time point. This procedure yielded an individual brain-state vector for each participant, which was compared with that obtained in the online EEG analysis that was performed in Experiments 1, 2, 3 and 4.

5.2.4.2. Temporal smoothing of network activity vector

Second, we applied essentially the same temporal smoothing to the binary vectors that represented each network activity in each individual (e.g., [1, –1, 1, 1, 1, …, 1] for the DMN activity in an individual). We applied the sliding-window-based smoothing to this network activity vector (window length = 10msec) and assigned the average activity in the window to each centre time point in the window as the representative network activity. Then, the vector of the average network activity underwent the same Gaussian smoothing filter (FWHM = 10msec). Finally, we binarised the smoothed vector (threshold = 0.5; active = 1, inactive = –1). These vectors were used when we evaluated the accuracy of the online EEG processing in Experiments 5 and 6.

5.3. Online analysis

The online EEG analysis was performed in all the BDNS experiments, and its procedure was essentially the same as that in the previous studies[36–39] and exactly the same as in our previous work[2]. First, we stated the online EEG analysis used for the BDNS in Experiments 2, 3 and 4; then we described a slightly different analysis procedure that was used in Experiments 5 and 6.

5.3.1. Preprocessing

We put the down-sampled EEG signals (<1.25kHz at 3kHz) to the real-time target PC machine through a DAQ board at 2kHz of sampling rate. The PC machine contained Simulink Real-Time model and xPC Target in Simulink (MathWorks, US), which analysed the EEG signals and triggered the TMS system via a TTL signal. We set an individual analysis model for each participant before the experiments.

First, each EEG signal was converted to a Hjorth signal using the neighbouring EEG signals at each time point. Next, we extracted the gamma-band signals (30-80Hz) in a sliding-window manner (window length = 1000msec) using a fast Fourier transformation (an upper panel of ***Extended Data Fig. 3***). As stated in **Section 5.2.1**, we focused on the gamma band of EEG signals since the gamma-band EEG dynamics were correlated with fMRI signals[31,34]. We then calculated the Hilbert envelope function for the gamma-band data; afterwards, to reduce the edge effects, we trimmed 100msec of the time-series data on both the edges of the time window[38,39], which resulted in an 800-msec neural signal for each electrode.

5.3.2. Prediction of EEG signals

Next, using these neural signals, we performed an autoregressive forward prediction based on Yule-Walker equation (order = 30)[2,36,38,39], which allowed us to infer 280msec of neural signals that would come after the edge of the trimmed data. In other words, considering the 100msec edge trimming, this calculation made a prediction on the neural signal between T = –100msec and T = 180msec when T = 0 was set at the actual recording timing (i.e., the original terminal edge of the EEG data; lower panel of ***Extended Data Fig. 3***).

The length of this forward prediction was set at 180msec since our previous BDNS study[2] successfully controlled brain state dynamics using the same parameter. In fact, this length of time window gave us a sufficient buffer for the following signal processing to realise a nearly simultaneous EEG-triggered TMS system[36].

These procedures yielded a 280-msec neural activity for each electrode.

5.3.3. Classification of electrodes

As in the offline analysis (**Section 5.2.2**), the electrodes were assigned to one of the nine brain networks based on the individual location map of the EEG electrodes. When an electrode was not located on any of the brain networks, we excluded its signal.

Based on this classification, for each network, we then averaged the 280-msec neural signals of the electrodes belonging to the network and obtained the mean network activity (***Extended Data Fig. 4***). Consequently, we obtained 280-msec time-series EEG data for each network in each participant around each time point.

5.3.4. Binarisation

We then binarised the neural signals in the 280-msec period. The binarisation threshold was calculated for each brain network based on the EEG data obtained in the first 5-min run of every BDNS experiment (***Extended Data Fig. 4***).

Precisely, we first applied the online preprocessing procedure (**Section 5.3.1**) to the down-sampled EEG data obtained during the first run of the BDNS experiment and obtained nine mean network activity vectors for the nine brain networks. We then calculated the temporal average of neural activity for each network and used the average values as the threshold of the binarisation of each network activity vector.

5.3.5. Brain state vector

Now, for each time point in the 280-msec window, we had a binary neural vector with nine elements. Next, we categorised each neural vector into one of the brain states based on the classification information that was obtained in the offline energy landscape analysis of the EEG data recorded in Experiment 1 (**Section 5.2.3**).

Next, to reduce the effects of signal fluctuation, we applied the same temporal smoothing protocol to the resultant brain state vector as those used in the offline analysis (**Section 5.2.4.1**), and obtained a series of representative brain states in a period between T = –95msec and T = 175msec (***Extended Data Fig. 4***).

5.3.6. Timing of TMS

Based on this temporally smoothed brain state vector, we determined the timing to trigger a train of TMS. In particular, we focused on the brain states that were predicted to dominantly appear in the forthcoming 150-msec period (from T = 25msec to T = 175msec; **Extended Data Fig. *5***).

As in our previous BDNS research[2], we administered the TMS only when we predicted that the target brain state would emerge dominantly in the forthcoming period (>90% in the time window). Technically, when the real-time analysis machine predicted such a case, the analysis machine sent a TTL trigger signal to the TMS device 21msec after the EEG signals were input to the real-time analysis machine.

We set this 21msec buffer for the online EEG analysis because the EEG data was supposed to take ~3msec to reach the real-time analysis machine and the TTL signal should take ~1msec to be delivered from the analysis machine to the TMS device. Given these latencies, the train of TMS was supposed to begin ~25msec after the EEG recording (i.e., T = 25msec).

In addition, the 21-msec buffer was long enough for the real-time EEG analysis. In fact, we confirmed this by connecting the TTL signal back to the DAQ board of the real-time analysis machine and measuring the signal processing delay. The delay ranged from 21.1msec to 21.6msec, which was close enough to 21msec.

Once a train of TMS was triggered, we did not administer the next train of TMS until at least 9sec passed from the last TMS, which enabled the BDNS to obtain a sufficient length of clean EEG data to calculate the timing of the next TMS. This 9-sec interval was the same as in our previous BDNS study[2].

5.3.7. Procedures for Experiments 5 and 6

The online EEG analysis for Experiments 5 and 6 was almost the same as that for the other experiments except for part of 'Brain state vector' (**Section 5.3.5**) and 'Timing of TMS' (**Section 5.3.6**).

In Experiments 5 and 6, we triggered the TMS simply based on the combination of the network activity. Therefore, we did not perform the brain state categorisation but used the binary neural vector with nine elements (i.e., nine brain networks) itself.

First, we rebuilt a binary network activity vector for each network (e.g., [1, 1, 1, –1, –1, 1, …–1] for the FPN; 1 for activity and –1 for inactive). Then, we applied the temporal smoothing used in the offline analysis (**Section 5.2.4.2**) to the vector to reduce the fluctuation. As a result, we obtained nine network activity vectors for each participant, which represented network-wise whole-brain activity in a time window from T = –95msec to T = 175msec.

Using these vectors, we determined the timing of TMS. Technically, as in Experiments 1-4, we focused on the period from T = 25msec to T = 175msec and triggered the TMS only when we predicted that the target activity pattern would emerge dominantly (>90% in the period). For example, in Experiment 5, we triggered the TMS when the VN would be active and the FPN would be inactive in most of the forthcoming 150-msec period.

For the other procedures and protocols, we adopted the same settings as in Experiments 1-4.

5.3.8. Dwelling time of brain states

This BDNS system implicitly assumed that, in most cases, the dwelling times of the brain states were longer than 150 msec. In fact, the analysis of the offline EEG data obtained in Experiment 1 validated this assumption: the averages of the median dwelling times for the four brain states were 6.5±0.8 sec (mean±std) for the major state #1, 6.3±0.9 sec for the major state #2, 3.2±0.3 sec for the minor state #1, and 3.0±0.4 sec for the minor state #2. These results were comparable to our previous observations on autistic brain dynamics[8].

6. TMS setting for BDNS

The current study adopted almost the same settings for TMS as in our previous BDNS research[2].

6.1. Excitatory TMS

As stated in the main manuscript, the numerical simulation indicated an excitatory stimulation as the optimal one. Therefore, we adopted a quadripulse TMS system, in which we could deliver a train of four monophasic magnetic pulses (200Hz) from the interconnected four magnetic stimulators (70mm-diameter double coil, DuoMag MP, DeyMed Diagnostic, Czech Republic). Therefore, on one occasion of the brain-state-driven trigger, we administered four 200Hz TMS pulses in 15 msec. Note that 20Hz four monophasic magnetic pulses were not adopted here since the TMS is considered to have inhibitory effects on the neural activity of the target brain region[2,6,40].

6.2. Magnitude of TMS

To reduce unpredicted neural effects on non-target sites, this BDNS did not use conventional quadripulse TMS (QPS) protocols[6,41–43], which often induce long-lasting after-effects on brain areas that are remote from the stimulated site[6,7]. Instead, we administered only one set of four TMS pulses in one stimulation and put ≥9-sec intervals between such stimulations. Moreover, we adopted a weaker TMS (70% of active motor threshold, AMT) than the conventional one (90% of AMT)[6,7]. We adopted the smaller magnitude of TMS since a previous study showed that, in EEG-triggered TMS systems, even such weak neural stimulation had sufficient neural effects[37], and another study demonstrated that brain-state-dependent TMS at this weak magnitude could induce significant behavioural changes[2].

The AMT was set as the lowest single-pulse TMS magnitude that could evoke a small response (>100μV) in more than half of the ten consecutive trials when the participants slightly contracted the right first dorsal interosseous (FDI) muscle (~10% of the maximum voluntary contraction). We recorded the MEPs of the right FDI with a pair of 9mm-diameter Ag/AgCl surface cup electrodes, which were placed over the muscle belly and the metacarpophalangeal joint of the right index finger[44]. We applied a temporal filter (100Hz–3kHz) to the MEP signals and searched for the optimal place for the stimulation of the right FDI muscle, over which the single-pulse TMS induced the largest MEP. This temporal filter was overlapped with those used in a line of other previous TMS studies (e.g., 100Hz-3kHz in ref [6,7,44] 150Hz-3kHz in ref [45]). The MEP signals were recorded at a sampling rate of 20kHz. The average AMT in the 50 ASD individuals was 33.1%±9.2% (mean±std) of the maximum stimulator output.

6.3. Location of TMS target region

The location of the TMS target was determined using a stereoscopic neuro-navigation system (Brainsight Neuronavigation, Rogue Research, UK). In each TMS session, we confirmed that the coil did not move throughout the experiment by comparing the locations of the TMS coil between the beginning and end of the TMS session. In fact, we did not find significant differences (<0.4cm) in any of the TMS sessions. Moreover, to avoid accidental dislocation during the sessions, the TMS coil was firmly set at a coil holder that was bespoke for the coil (BrainBox Ltd, UK). That is, it is reasonable that the TMS coil was not dislocated during the experiments.

6.4. Number of TMS administration

In Experiment 3, we performed the BDNS during the major state #1. In this setting, we administered 30.5±4.1 (mean±std) times in a 5-min run. In Experiment 4, the TMS was triggered during the major state #1, which was observed 29.5±4.8 times in a 5-min run. In Experiment 5, we administered the TMS when the FPN was inactive but the VN was inactive, whose frequency was 34.5±5.3 times in a 5-min run. In Experiment 6, the TMS was triggered when the FPN was inactive but both the DMN and SAN were active, whose frequency was 28.9±4.2 times in a 5-min run.

7. Settings for conventional 30-min rTMS

To compare the current BDNS protocol to the conventional TMS protocol, we examined the neural effect of 30-min excitatory repetitive TMS (rTMS) over the SPL, whose protocol was the same as that we adopted in our previous studies[6,7]. In the rTMS session, we administered 360 consecutive bursts with 5-sec intervals, in which each burst consisted of four monophasic 200Hz TMS (90% of AMT). During the session, the participants were asked to rest with their eyes open. The individual neural effect was calculated based on the rsfMRI data obtained before and after this rTMS/sham session.

8. Details of numerical simulation

To identify the optimal BDNS condition, we numerically examined how the TMS affected the structures of the individual energy landscape and, resultantly, the brain state dynamics on it. We performed this simulation essentially the same manner as in our previous study[2]. Note that we performed all the simulation based on the energy landscape built from the rsfMRI data collected in Experiment 1.

8.1. Simulation of effects of excitatory TMS

If Network$_i$ (i = 1, … , 9) was the target site of the excitatory TMS, we removed all the binary neural vectors, V^t, whose element i, σ_i, was set at –1 (i.e., inactive), from the energy landscape. Then, we re-built the disconnectivity graph and estimated the structural properties of the energy landscape (see **Section 4.3.5**). When any local minimum representing any brain state was removed in the first place, we alternatively used the brain state that included the neighbouring neural vector as the brain state.

We repeated this simulation for all the nine networks in all the participants.

8.2. Simulation of effects of inhibitory TMS

The neural effects of the inhibitory TMS were simulated in almost the same procedure as those of the excitatory TMS. In this case, if Network$_i$ was the target site of the inhibitory TMS, we removed all the binary neural vectors, V^t, whose element i, σ_i, was set at 1 (i.e., active), from the energy landscape. Afterwards, we conducted the same calculation as in **Section 8.1**.

9. Additional Experiments

In Experiments 4–6, we demonstrated the significant behavioural effects of the BDNS compared to the sham condition, in which the participants experienced the same acoustic stimuli as in the BDNS condition. To examine the robustness of this observation, we performed three additional experiments with a new control condition (Additional Experiments 1–3; **Supplementary Fig. 10a**): in the new control, the participants experienced the same excitatory TMS over the same right SPL area as in the original BDNS condition but at random timings. Thus, differently from the BDNS that was designed to trigger a TMS only during the major state #1, we administered a series of TMS with random intervals without considering brain state dynamics.

9.1. Experiment design

Mainly due to the difficulty in the continual recruits of the same participants, we did not adopt a cross-over design for the three additional experiments but a randomised control design.

Additional Experiment 1 was conducted to examine the robustness of the results of Experiment 4, whereas Additional Experiments 2 and 3 were set to assess the reproducibility of the results of Experiments 5 and 6, respectively. We shortened the lengths of these additional longitudinal experiments since the original experiments already pointed out how many BDNS sessions should be repeated to induce significant behavioural changes. That is, except for the new control conditions, Additional Experiment 1 was an 8-week version of Experiment 4, whereas Additional Experiments 2 and 3 were 2-week versions of Experiments 5 and 6, respectively.

In each BDNS condition, the participants underwent exactly the same BDNS protocol as in each corresponding main experiment.

9.2. Random-timing TMS condition

In the random-timing TMS condition, the TMS intervals were determined based on individual records observed in the BDNS session in the last week in the corresponding experiment.

For example, for Additional Experiment 1, we first calculated the TMS intervals (inter-stimulation intervals, ISIs) observed in Week 13 in Experiment 4 for each individual. Then, we randomised the order of the TMS intervals and administered a train of TMS based on the individually randomised intervals.

In the same logic, the ISIs in Additional Experiment 2 were set at a randomised sequence of the ISIs observed in Week 7 of Experiment 5, and those in Additional Experiment 3 were defined by a randomised sequence of the ISIs seen in Week 7 of Experiment 6.

9.3. Participants

We first re-recruited the same 40 high-functioning autistic individuals who completed the 12-week longitudinal experiment (Experiment 4) for the three additional experiments and then randomly assigned the 40 ASD adults to the following two groups (**Supplementary Fig. 10a**): 20 for Additional Experiment 1 and the other 20 for Additional Experiments 2 and 3.

The former 20 autistic adults were then randomly assigned to the 8-week weekly BDNS session or 8-week weekly random-timing TMS session. The latter 20 were first randomly assigned to Additional Experiment 2 or 3. Then, they were randomly split into 10 who underwent the BDNS session and 10 who underwent the random-timing TMS session. After completion of one of Additional Experiments 2 and 3, they were given a ≥2-week wash-out period. Then, they were assigned to the other Additional Experiment, in which randomly-selected 10 participants underwent the BDNS session and the other 10 adults the random-timing TMS session.

10. Statistics

10.1. Multiple Comparisons

Multiple comparisons were corrected in a Bonferroni manner as follows:

- Comparisons of four brain states between TD and ASD (Fig. 2a and 2l): corrected between the four brain states; $\alpha = 0.05/4$.
- Correlations between the indirect transition frequency and autistic behaviours (Fig. 2e-2h and 2n): corrected between ASD clinical score and three experiment measures; $\alpha = 0.05/4$.
- Correlations between two autistic behavioural indices and ADOS sub-scores (Fig. 2j and 2k): corrected between the two indices; $\alpha = 0.05/2$.
- Brute-force numerical simulation to identify the target brain network (Fig. 3b): corrected between the nine networks in the two conditions; $\alpha = 0.05/18$.
- Comparisons of brain state transition frequency (Fig. 3e and 3f): corrected between the two conditions (baseline v FPN+); $\alpha = 0.05/2$.
- Comparisons of the neural effects between the different BDNS conditions (Fig. 3i): corrected between the three BDNS target regions; $\alpha = 0.05/3$.
- Comparisons of the neural effects between the different BDNS conditions (Fig. 3j): corrected between the four BDNS target brain states; $\alpha = 0.05/4$.
- Evaluation of the longitudinal effects of the BDNS (Fig. 4e-4h): corrected between the 13 recording points for the neural effect and between seven recording points for the behavioural effects; $\alpha = 0.05/13$ for the neural effect, $\alpha = 0.05/7$ for the behavioural effects.
- Comparisons of the dwelling times of the two minor states between the TD and ASD groups (Fig. 5b): corrected between the two states; $\alpha = 0.05/2$.
- Prolongation of the dwelling times of the two minor states throughout the BDNS sessions (Fig. 5c): corrected between the 13 BDNS sessions; $\alpha = 0.05/13$.

- Correlations between the changes in the dwelling times of the minor states and those in the indirect transition frequency in the longitudinal BDNS experiment (Fig. 5d): corrected between the 13 BDNS sessions; $\alpha = 0.05/13$.
- Correlations between the change in the network coupling strength and that in percept duration (Fig. 5i): corrected between the seven recording points; $\alpha = 0.05/7$.
- Correlation between the change in the dwelling times of the minor states and that in the FPN-VN coupling (Fig. 5l): corrected between the 13 BDNS sessions; $\alpha = 0.05/13$.
- Mediation effects (Fig. 5n and 5o): corrected between seven weeks (Week 7 to 13); $\alpha = 0.05/7$.
- The neural effects in Experiment 5 (Fig. 6b): corrected between the seven BDNS sessions; $\alpha = 0.05/7$.
- The behavioural effects in Experiment 5 (Fig. 6c): corrected between the four recording points: $\alpha = 0.05/4$.
- Correlation between the network coupling strength and NVJ (Fig. 7c): corrected between 8 pairs of networks; $\alpha = 0.05/8$.
- Correlation between the network coupling strength and NVJ (Fig. 7b and 7d): corrected between 36 triads of networks; $\alpha = 0.05/36$.
- Correlations between the network coupling strength and NVJ proportion throughout the experiment: corrected between the seven recording points (Fig. 7e and 7f): corrected between the seven recording points; $\alpha = 0.05/7$.
- Correlations between the duration of brain state and network coupling strength (Fig. 7g): corrected the 13 recording time points; $\alpha = 0.05/13$.
- Mediation effects (Fig. 7h and 7i): corrected between the five recording points; $\alpha = 0.05/5$.
- Mediation effects (Fig. 7j): corrected between the three recording points; $\alpha = 0.05/3$.
- The effects on the network coupling strength (Fig. 8b): corrected between the six recording points; $\alpha = 0.05/6$.
- The behavioural effects (Fig. 8c): corrected between the four recording points; $\alpha = 0.05/4$.
- The behavioural effects in Additional Experiment 1: corrected between the eight recording points; $\alpha = 0.05/8$.
- The neural and behavioural effects in Additional Experiments 2 and 3: corrected between the two recording points; $\alpha = 0.05/2$.

10.2. Mediation analysis

All the mediation analyses were performed after confirming significant correlations for all the pairs between the independent variable, mediator variable(s) and dependent variable.

Supplementary References

1. Watanabe, T., Lawson, R. P., Walldén, Y. S. E. & Rees, G. A Neuroanatomical Substrate Linking Perceptual Stability to Cognitive Rigidity in Autism. *J Neurosci* **39**, 6540–6554 (2019).

2. Watanabe, T. Causal roles of prefrontal cortex during spontaneous perceptual switching are determined by brain state dynamics. *Elife* **10**, e69079 (2021).

3. Martino, A. D. *et al.* The autism brain imaging data exchange: towards a large-scale evaluation of the intrinsic brain architecture in autism. *Mol Psychiatr* **19**, 659–667 (2014).

4. Lord, C. *et al.* Austism diagnostic observation schedule: A standardized observation of communicative and social behavior. *J Autism Dev Disord* **19**, 185–212 (1989).

5. Rossi, S., Hallett, M., Rossini, P. M., Pascual-Leone, A. & Group, T. S. of T. C. Safety, ethical considerations, and application guidelines for the use of transcranial magnetic stimulation in clinical practice and research. *Clin Neurophysiol* **120**, 2008–2039 (2009).

6. Watanabe, T. *et al.* Bidirectional effects on interhemispheric resting-state functional connectivity induced by excitatory and inhibitory repetitive transcranial magnetic stimulation. *Hum. Brain Mapp.* **35**, 1896–1905 (2014).

7. Watanabe, T. *et al.* Effects of rTMS of Pre-Supplementary Motor Area on Fronto Basal Ganglia Network Activity during Stop-Signal Task. *J Neurosci* **35**, 4813–4823 (2015).

8. Watanabe, T. & Rees, G. Brain network dynamics in high-functioning individuals with autism. *Nat Commun* **8**, 16048 (2017).

9. Power, J. D. *et al.* Functional Network Organization of the Human Brain. *Neuron* **72**, 665–678 (2011).

10. Arrington, C. M. & Logan, G. D. The Cost of a Voluntary Task Switch. *Psychol Sci* **15**, 610–615 (2003).

11. Poljac, E., Poljac, E. & Yeung, N. Cognitive Control of Intentions for Voluntary Actions in Individuals With a High Level of Autistic Traits. *J Autism Dev Disord* **42**, 2523–2533 (2012).

12. Poljac, E. *et al.* Impaired task switching performance in children with dyslexia but not in children with autism. *Q J Exp Psychology* **63**, 401–416 (2010).

13. Watanabe, T., Masuda, N., Megumi, F., Kanai, R. & Rees, G. Energy landscape and dynamics of brain activity during human bistable perception. *Nat Commun* **5**, 4765 (2014).

14. Robertson, C. E., Kravitz, D. J., Freyberg, J., Baron-Cohen, S. & Baker, C. I. Slower Rate of Binocular Rivalry in Autism. *J Neurosci* **33**, 16983–16991 (2013).

15. Freyberg, J., Robertson, C. E. & Baron-Cohen, S. Reduced perceptual exclusivity during object and grating rivalry in autism. *J Vision* **15**, 11 (2015).

16. Robertson, C. E., Ratai, E.-M. & Kanwisher, N. Reduced GABAergic Action in the Autistic Brain. *Curr Biol* **26**, 80–85 (2016).

17. Watanabe, T. *et al.* Clinical and neural effects of six-week administration of oxytocin on core symptoms of autism. *Brain* **138**, 3400–3412 (2015).

18. Watanabe, T. *et al.* Diminished Medial Prefrontal Activity behind Autistic Social Judgments of Incongruent Information. *Plos One* **7**, e39561 (2012).

19. Watanabe, T. *et al.* Mitigation of Sociocommunicational Deficits of Autism Through Oxytocin-Induced Recovery of Medial Prefrontal Activity: A Randomized Trial. *Jama Psychiat* **71**, 166–175 (2014).

20. Watanabe, D. & Watanabe, T. Distinct Frontoparietal Brain Dynamics Underlying the Co-Occurrence of Autism and ADHD. *eNeuro* **10**, ENEURO.0146-23.2023 (2023).

21. Watanabe, T. *et al.* A pairwise maximum entropy model accurately describes resting-state human brain networks. *Nat Commun* **4**, 1370 (2013).

22. Ezaki, T., Sakaki, M., Watanabe, T. & Masuda, N. Age-related changes in the ease of dynamical transitions in human brain activity. *Hum. Brain Mapp.* **39**, 2673–2688 (2018).

23. Schneidman, E., Berry, M. J., Segev, R. & Bialek, W. Weak pairwise correlations imply strongly correlated network states in a neural population. *Nature* **440**, 1007–1012 (2006).

24. Ganmor, E., Segev, R. & Schneidman, E. The Architecture of Functional Interaction Networks in the Retina. *J Neurosci* **31**, 3044–3054 (2011).

25. Shlens, J. *et al.* The Structure of Multi-Neuron Firing Patterns in Primate Retina. *J Neurosci* **26**, 8254–8266 (2006).

26. Tang, A. *et al.* A Maximum Entropy Model Applied to Spatial and Temporal Correlations from Cortical Networks In Vitro. *J. Neurosci.* **28**, 505–518 (2008).

27. Kang, J., Pae, C. & Park, H.-J. Energy landscape analysis of the subcortical brain network unravels system properties beneath resting state dynamics. *Neuroimage* **149**, 153–164 (2017).

28. Jeong, S.-O. *et al.* Empirical Bayes estimation of pairwise maximum entropy model for nonlinear brain state dynamics. *Neuroimage* **244**, 118618 (2021).

29. Girvan, M. & Newman, M. E. J. Community structure in social and biological networks. *Proc National Acad Sci* **99**, 7821–7826 (2002).

30. Massen, C. P. & Doye, J. P. K. Identifying communities within energy landscapes. *Phys Rev E* **71**, 046101 (2005).

31. Watanabe, T., Rees, G. & Masuda, N. Atypical intrinsic neural timescale in autism. *Elife* **8**, e42256 (2019).

32. Delorme, A. & Makeig, S. EEGLAB: an open source toolbox for analysis of single-trial EEG dynamics including independent component analysis. *J Neurosci Meth* **134**, 9–21 (2004).

33. Hyvärinen, A., Ramkumar, P., Parkkonen, L. & Hari, R. Independent component analysis of short-time Fourier transforms for spontaneous EEG/MEG analysis. *Neuroimage* **49**, 257–271 (2010).

34. Deligianni, F., Centeno, M., Carmichael, D. W. & Clayden, J. D. Relating resting-state fMRI and EEG whole-brain connectomes across frequency bands. *Front Neurosci-switz* **8**, 258 (2014).

35. Hjorth, B. EEG analysis based on time domain properties. *Electroen Clin Neuro* **29**, 306–310 (1970).

36. Chen, L. L., Madhavan, R., Rapoport, B. I. & Anderson, W. S. Real-Time Brain Oscillation Detection and Phase-Locked Stimulation Using Autoregressive Spectral Estimation and Time-Series Forward Prediction. *Ieee T Bio-med Eng* **60**, 753–762 (2013).

37. Schaworonkow, N., Triesch, J., Ziemann, U. & Zrenner, C. EEG-triggered TMS reveals stronger brain state-dependent modulation of motor evoked potentials at weaker stimulation intensities. *Brain Stimul* **12**, 110–118 (2019).

38. Stefanou, M.-I., Desideri, D., Belardinelli, P., Zrenner, C. & Ziemann, U. Phase Synchronicity of μ-Rhythm Determines Efficacy of Interhemispheric Communication Between Human Motor Cortices. *J. Neurosci.* **38**, 10525–10534 (2018).

39. Zrenner, C., Desideri, D., Belardinelli, P. & Ziemann, U. Real-time EEG-defined excitability states determine efficacy of TMS-induced plasticity in human motor cortex. *Brain Stimul.* **11**, 374–389 (2018).

40. Hamada, M. *et al.* Quadro-pulse stimulation is more effective than paired-pulse stimulation for plasticity induction of the human motor cortex. *Clin Neurophysiol* **118**, 2672–2682 (2007).

41. Hamada, M. *et al.* Primary motor cortical metaplasticity induced by priming over the supplementary motor area. *J Physiology* **587**, 4845–4862 (2009).

42. Seeck, M. *et al.* The standardized EEG electrode array of the IFCN. *Clin Neurophysiol* **128**, 2070–2077 (2017).

43. Shirota, Y. *et al.* Influence of Short-Interval Intracortical Inhibition on Short-Interval Intracortical Facilitation in Human Primary Motor Cortex. *J Neurophysiol* **104**, 1382–1391 (2010).

44. Hanajima, R. *et al.* Interhemispheric facilitation of the hand motor area in humans. *J Physiology* **531**, 849–859 (2001).

45. Osada, T. *et al.* An Essential Role of the Intraparietal Sulcus in Response Inhibition Predicted by Parcellation-Based Network. *J. Neurosci.* **39**, 2509–2521 (2019).

46. Ezaki, T., Watanabe, T., Ohzeki, M. & Masuda, N. Energy landscape analysis of neuroimaging data. *Philosophical Transactions Royal Soc Math Phys Eng Sci* **375**, 20160287 (2017).